SAND2021-15770C

Towards Structured PLIF Excitation for Probing Harsh Environments

Joshua W. Hargis[1], William E. Swain[2], Daniel R. Guildenbecher[3], Sean P. Kearney[4], and Daniel R. Richardson[5]

Sandia National Laboratories, Albuquerque, NM, 87185, USA

Planar laser induced fluorescence is a common diagnostic technique employed in the probing of flames and other combustion phenomena. In this work, structured illumination is coupled to the application of OH PLIF in a Hencken burner to demonstrate its utility for single-camera, single snapshot background subtraction. This variant of structured PLIF illumination is being developed for eventual application to transient environments where background radiation cannot be quantified from ensemble averaging. The extension of the structured illumination signal (in the recorded PLIF image) to multiple spatial frequencies is also demonstrated with potential utility for multi-wavelength PLIF thermometry.

1. Introduction

When performing optical diagnostic measurements in combustion environments with the PLIF technique, background subtraction is often a necessary analysis step. However, such a procedure is often difficult, if not impossible, to perform in environments with highly transient phenomena where significant background radiation exists, such as in luminous turbulent flames or detonation environments [1-5]**.** One technique to filter out background radiation in harsh environments is the utilization of structured illumination coupled to the application of spatial Fourier transform space [6-20]. Such an alternative to conventional background subtraction provides access to diagnostics previously unattainable in highly transient environments with large amounts of background luminosity, two-color PLIF thermometry, in particular. In this paper, the mechanics of employing the structured illumination technique are discussed. Additionally, structured illumination is applied to PLIF data collected from a Hencken burner and the data are analyzed with and without background subtraction. Further discussion of extending the applicability of the spatial Fourier transform technique to multiple spatial frequencies is then provided. A brief discussion on improving the quality of the recorded data is also given. Lastly, we provide a discussion of the application of the technique to two-color OH PLIF thermometry with some preliminary results using conventional thermometry as part of future work.

2. Experimental Setup

The basic experimental setup utilized herein is similar to other standard PLIF apparatuses [21-24]. A 10 Hz Nd:YAG laser (Spectra Physics Pro350) with a 1064 nm fundamental wavelength which is frequency doubled to 532 nm serves as a pump source for a Rhodamine dye laser (Sirah PrecisionScan) with a tunable output around 560 nm. This dye laser output is frequency doubled via an integrated frequency conversion unit, within the Sirah dye laser, in the range of 281-287nm. This UV-wavelength output beam is then used to excite various rovibrational transitions in the OH spectrum in a Hencken burner H_2-Air flame. In this work, the UV radiation was emitted at 282.75 nm and 286.46 nm corresponding to the $Q_1(5)$ and $Q_1(14)$ lines, respectively, of the (1,0) band of the OH $A^2\Sigma$-$X^2\Pi$ electronic transition. To image the fluorescence radiation, a Princeton Instruments PI-MAX 4 Intensified CCD (ICCD) camera was placed perpendicular to the propagation direction of the PLIF sheet. One key difference of the PLIF setup described herein and that of canonical

[1] Postdoctoral Appointee, Engineering Sciences Center, jwhargi@sandia.gov, AIAA Member.
[2] Senior Test Operations Engineer, Engineering Sciences Center.
[3] Principal Member of the Technical Staff, Diagnostic Science and Engineering, AIAA Senior Member.
[4] Distinguished Member of the Technical Staff, Diagnostic Science and Engineering, AIAA Associate Fellow.
[5] Senior Member of the Technical Staff, Diagnostic Science and Engineering, AIAA Senior Member.

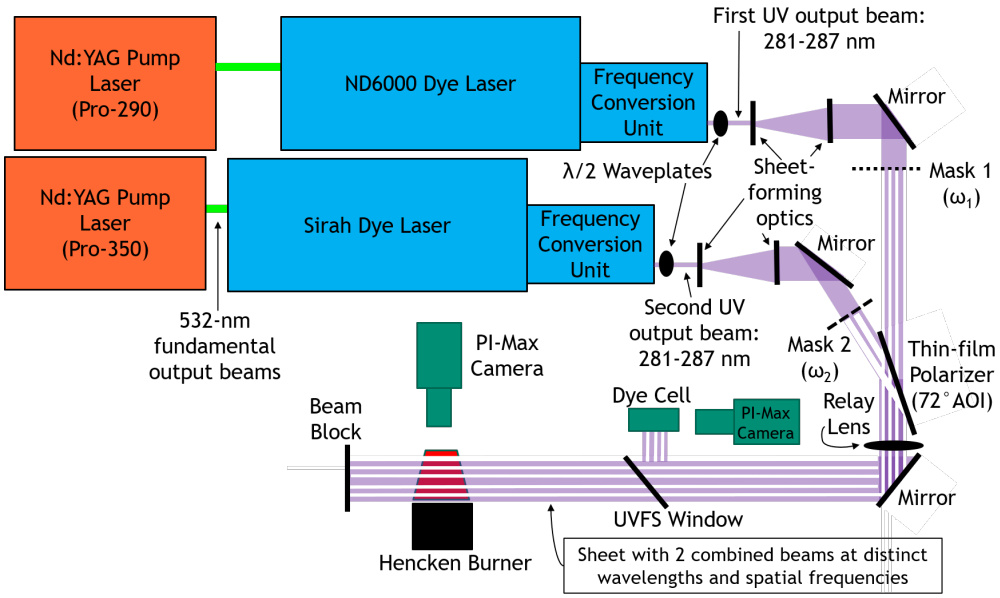

Figure 1. OH PLIF optical setup configured for two channels incorporating structured illumination.

PLIF diagnostics is the use of a mask to impose a known 1D intensity pattern on the excitation laser sheet. This results in a PLIF image with a periodic vertical frequency component (horizontal striped appearance of the PLIF sheet) and is often referred to as structured illumination. Such an imposed frequency does in fact limit some of the information that can be collected within the measurement volume (limits vertical resolution). However, background subtraction using multiple sets of images (typically done by recording and averaging PLIF data over a series of shots, then repeat the same recording without the PLIF sheet) is not necessary. This technique is advantageous for measurements conducted in environments where background subtraction is difficult or altogether impossible and will be discussed in further detail throughout this paper.

An additional advantage of the structured illumination technique is that it is not limited to a single input laser beam and associated PLIF sheet as is typically the case for methods which do not employ structured illumination [8, 9, 17, 25, 26]. For the work performed herein, the basics of the technique are demonstrated using both a single structured PLIF laser sheet and two structured PLIF laser sheets, resulting in two PLIF measurement channels on a single detector. With the benefits of performing signal filtering in the Fourier plane, more than two measurement channels can of course be incorporated into a given setup. However, the application of interest, which is discussed later, requires only two measurement channels. The experimental setup used in this work for either single or two-channel OH PLIF measurements is given in Figure 1. Similar to the first laser system, the second laser system consists of a pump laser (SpectraPhysics Pro-290) coupled to a tunable Rhodamine dye laser (Continuum ND6000) which feeds a frequency conversion unit for frequency-doubling the dye laser output.

Compared to many of the references contained herein, the current setup combines the propagation vectors of each laser sheet in a colinear fashion rather than the sheet propagation vectors being incident upon the measurement volume at different angles. Reasons for choosing this configuration are discussed in a following section. To combine each laser sheet, a set of half-wave plates are coupled with a thin film polarizer such that each sheet contains a different polarization, allowing one sheet to pass through the polarizer with the other being reflected off the polarizer, resulting in co-propagating beams each with a distinct wavelength and structure frequency. It should also be noted that the setup incorporates a relay lens system. The incorporation of structured illumination necessitates that the laser sheet be focused at the mask plane and then re-imaged at the measurement volume. In some instances, a knife edge may be needed to eliminate stray reflections from the thin-film polarizer, in which case an additional relay optic can be incorporated in the system such that the mask plane is imaged once downstream to the knife edge and then again at the measurement volume. Lastly, a window is placed just upstream of the measurement volume such that a small amount of the beam is reflected into a dye cell for imaging the sheet profile on a separate camera (PI-Max II) and performing sheet profile corrections in post-processing.

3. Structured Illumination: Technique Basics, Background Subtraction, and Multi-Channel Imaging

Aside from the obvious physical differences of integrating the structured illumination technique into a standard PLIF hardware setup, the analysis performed on PLIF data incorporating structured illumination is also different. An example graphic depicting the various steps in the analysis process of extracting data from structured PLIF sheets is given in Figure 2. All raw PLIF sheet images displayed herein are the average of 100 exposures, with each camera exposure capturing the fluorescence from a single laser pulse. The exposure time of the camera was set to 10 ns with a record rate of 10 Hz and a gain on the intensifier of 54, with the laser wavelength set at 282.75 nm. In frame a), the raw data from a structured PLIF image using a single laser sheet from the setup shown in Figure 1 is given (only one of the two laser shutters is open). A 2-D spatial Fourier transform is then applied to the data, and for the purposes of visualizing the peaks the complex magnitude of each pixel of data is also taken, all shown in frame b) of Figure 2. It is important to note that identical sets of information are recorded in frame a) and frame b) of Figure 2. Frame b), however, is showing the magnitude of the image as represented in the Fourier plane. Using the Fourier-processed data, a Gaussian filter is applied to the image from frame b) such that the region containing the frequency of interest (the information from the PLIF sheet with the imposed spatial frequency in frame a)) is kept while other data are discarded. This is highlighted in frame c) by zooming-in to the regions of interested from frame b). With the application of the Gaussian filter, from frame c), the inverse Fourier transform is applied to that data and the un-masked PLIF image is displayed.

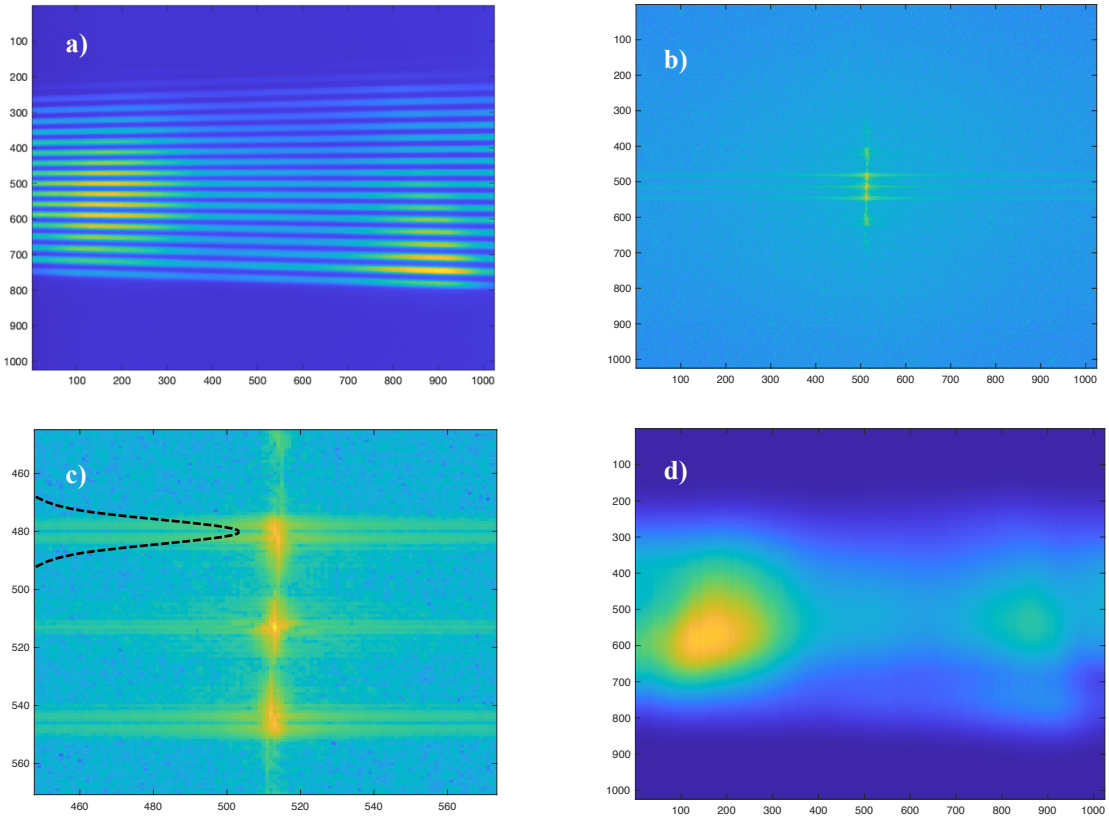

Figure 2. Analysis method for PLIF data in structured illumination experiments. a) PLIF image resultant from inclusion of a mask in the setup, b) Magnitude of 2D Fourier transform of image in frame a), c) Zoomed view of frame b) showing region of interest for Gaussian filter, d) Resultant PLIF image after taking inverse 2D Fourier transform (and magnitude) of data from Gaussian-selected data in frame c).

In practice, harsh environments, such as those occurring in turbulent flames [27, 28] or even post-detonations fireballs [29, 30], will require short exposure times due to the highly transient nature of the flow field whilst still emitting large amounts of background radiation. These challenges make the technique discussed herein essential to collecting meaningful quantitative data in environments where conventional background subtraction is not possible. As a demonstration of the utility of the technique for applications in harsh environments, various PLIF images were recorded, and Fourier analysis performed for conditions where significant amounts of background radiation were present. Such conditions were simulated by setting the exposure time on the camera to 500 ms.

For the demonstration of background filtering, two forms of data collection and analysis were conducted. While both sets of analysis were performed utilizing the structured illumination technique, only one involved background subtraction. In the first set of data, shown in Figure 3a, a structured PLIF image was recorded using the long camera gate time of 500 ms. The background image recorded at an equivalent gate time (frame b) was then subtracted from the primary signal image to yield the structured PLIF signal to be analyzed (frame c). After background subtraction, the previously discussed Fourier transform analysis was performed on the background subtracted structured PLIF image, resulting in the processed PLIF image shown in frame d) of Figure 3.

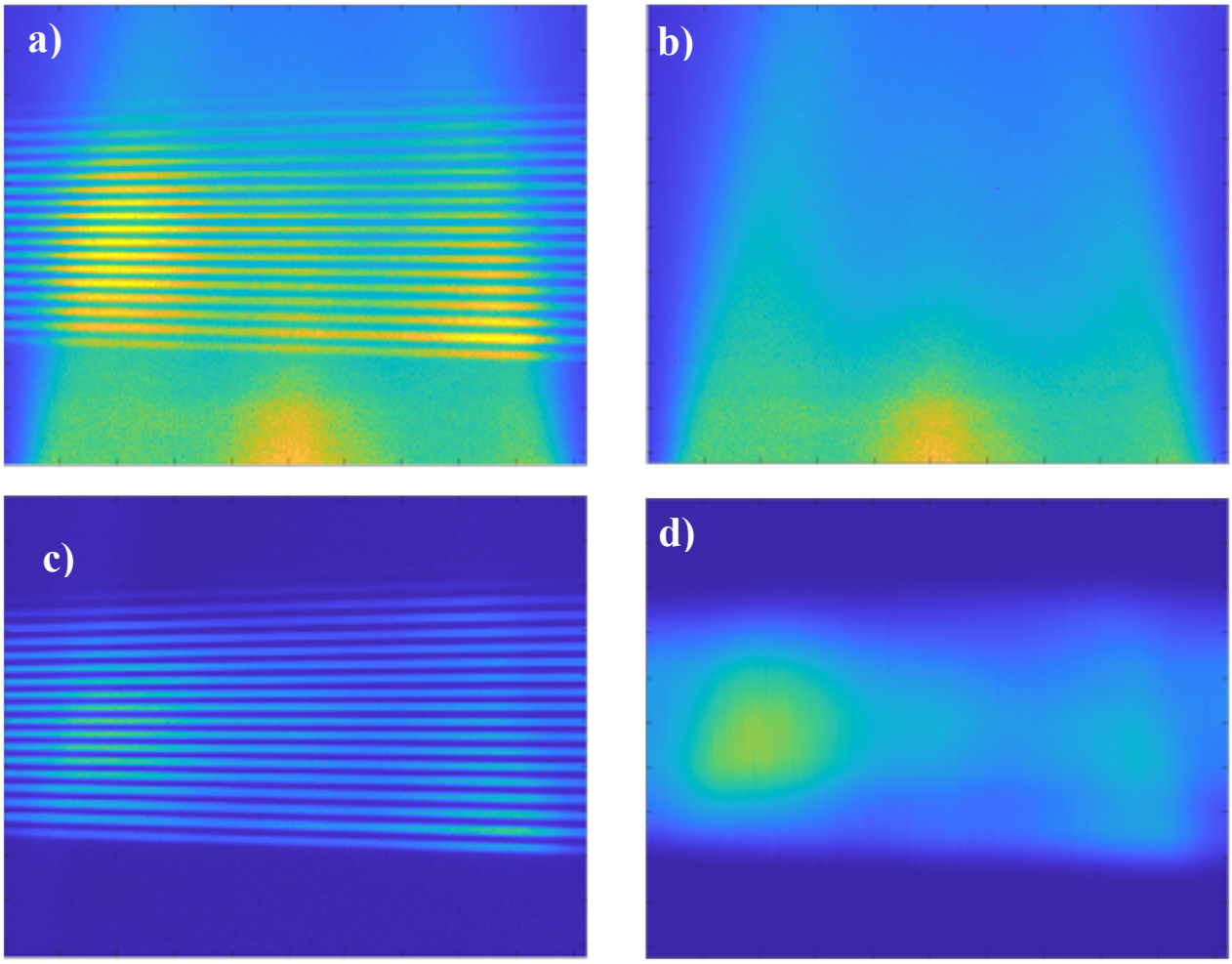

Figure 3. Images taken at a camera exposure time of 500 ms and analyzed with the 2D Fourier transform method. All frames have dimensions of 1024 pixel x 1024 pixels. a) Structured PLIF signal with background, b) Background image (laser turned off), c) Background-subtracted image (subtract frame b from frame a), d) PLIF sheet from 2D Fourier analysis of frame c). Frames a)-c) are equivalently scaled, but frame d) has had its contrast enhanced relative to the other frames to better view the resultant PLIF sheet.

Similar to the Fourier analysis performed on the image in Figure 3a which included background subtraction, the 2D Fourier analysis was performed on the same image, this time without background subtraction. The results of the analysis are shown in Figure 4. Comparing the results within the 2 figures shows very similar results between frame d) of Figure 3 and frame b) of Figure 4. One noticeable difference is the smearing of information vertically in the results of the analysis in Figure 4. This is primarily due to two factors. First, the choice of filter (Gaussian) and filter parameters (location, width) affect how finely the various spatial frequencies can be separated. Second, the choice of spatial frequency and its proximity to the zero frequency affects the ability to filter out information other than the desired spatial frequency. Note in Figure 2c that the spatial frequency resultant from the chosen mask in the PLIF setup is relatively close in frequency space to the zero frequency (DC) location. Were the mask in the PLIF setup to have finer graduations, then the location of the desired frequency in Figure 2c would be further away from the zero-frequency location and filtering of the image is likely to result in improved signal to noise.

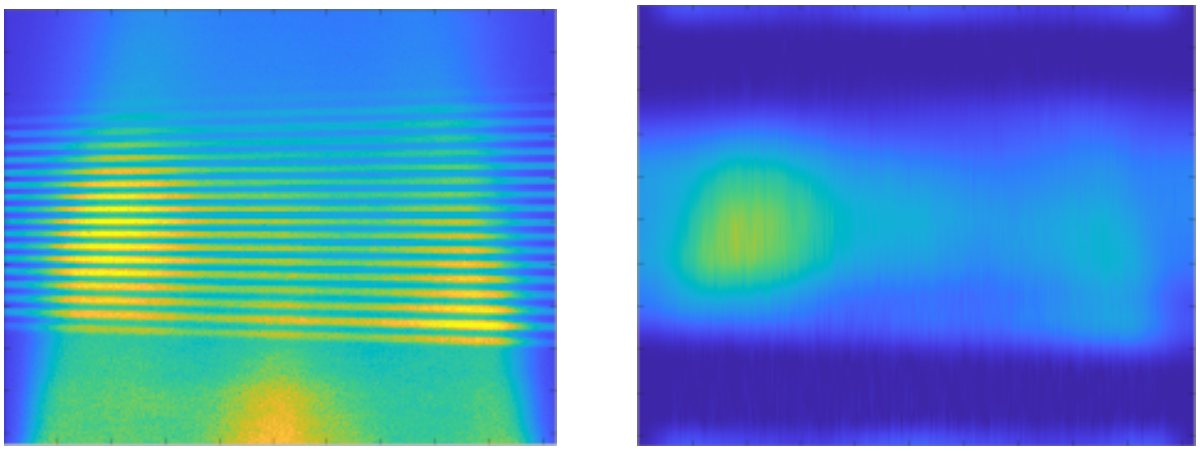

Figure 4. Removal of unstructured background radiation via single shot structured PLIF. The right-hand frame in this figure has been equivalently scaled to that of frame d) from Figure 3.

As discussed previously, incorporating structured illumination when probing harsh environments provides experimenters with the ability to filter out unwanted background radiation. A natural extension of the technique is to apply multiple diagnostics with distinct spatial frequencies to the probe volume and separate them using similar analysis as that which was performed in Figure 2. Thus, a single image can in fact incorporate multiple channels of measurement data even when only a single camera is employed. Consider frame b) of Figure 2. The 2D Fourier transform resultant in this image shows that 2 spatial frequencies largely dominate the signal present in the original image (frame a)); the zero-frequency signal (the background signal) located in the center of the image and the imposed spatial frequency from the mask in the PLIF beam offset from center (note that this is displayed in Fourier space as 2 distinct peaks since real signals contain both positive and negative frequency components – see the Euler formula). Were other spatial frequencies overlayed on the PLIF signal they would be separated and appear in different locations in the Fourier plane. Subsequent Gaussian (or other types) of filtering to select only the desired signal(s) can then be applied to separate the resultant PLIF images for each of the spatial frequencies present in the original PLIF image. Thus, multiple channels of information can be extracted from a single PLIF camera image. To demonstrate the utility of multi-channel structured illumination to the application of OH-PLIF, a two-channel measurement was performed using both of the laser systems shown in Figure 1.

Using the 2-channel structured illumination optical setup shown in Figure 1, 2 sets of OH PLIF data were recorded. For simplicity, all data in this analysis were recorded with the lasers set at a wavelength of 282.75 nm. First, a reference set of data from each laser system was recorded: a series of OH PLIF images of the Hencken burner were captured using the Sirah dye laser beam, and then a series of images using the ND6000 dye laser beam, each with no masks. These conventional OH PLIF images serve as a reference by which to compare OH PLIF data recorded using the structured illumination technique. After the reference images were recorded, a set of images were recorded using both lasers

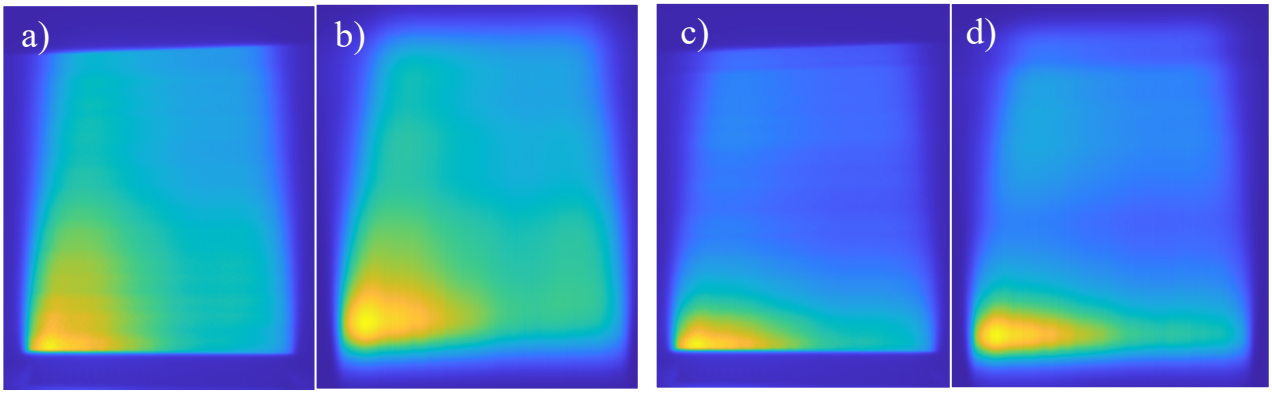

Figure 5. Comparison of standard OH PLIF images and OH PLIF images extracted using the two-channel structured illumination Fourier processing technique. Frames a) and b) are the reference and Fourier-processed OH PLIF sheet images, respectively, from the Sirah laser system. Frames c) and d) are the reference and Fourier-processed OH PLIF sheet images, respectively, from the ND6000 laser system.

simultaneously in conjunction with the structured illumination technique, after which the individual laser sheet images were extracted in post-processing.

The reference data recorded separately for each PLIF sheet are given in Figure 5, frames a) and c), as are the post-processed data extracted from the structured illumination images. Each reference image was corrected for background signal and for flat-field non-uniformities. The 2-channel data recorded simultaneously with the structured illumination PLIF sheets are also given in Figure 5. In comparing the reference and post-processed structured illumination data, it is observed that the general shape and intensity profiles of the flames are maintained between the reference data and structured illumination data. While some resolution is lost due to the incorporation of the mask in the optical setup (see Figure 1), this is to be expected and will be discussed further in the discussion section and in the section regarding future work.

4. Discussion of the Structured Illumination Technique

As mentioned in the section detailing the experimental setup, the two PLIF laser sheets formed have colinear propagation vectors. In the numerous works utilizing structured illumination referenced herein, the propagation vectors are often incident upon the probe volume in directions perpendicular to one another, or at least with significant angles between them. Such is not the case with the setup described here. The choice of aligning the propagation vectors of the two laser sheets was motivated by the type of environment to be probed. As part of future work (discussed later), the diagnostic described herein is being developed for application to imaging a post-detonation fireball environment. Laboratory scale experiments that contain such events have strict safety tolerances and limits to optical access (particularly for windows large enough to accommodate PLIF optics), thereby limiting the number of optical access ports for both propagation and observation of a PLIF sheet. Thus, as a first iteration in the experimental setup, it was decided to co-align the propagation vectors of both PLIF sheets.

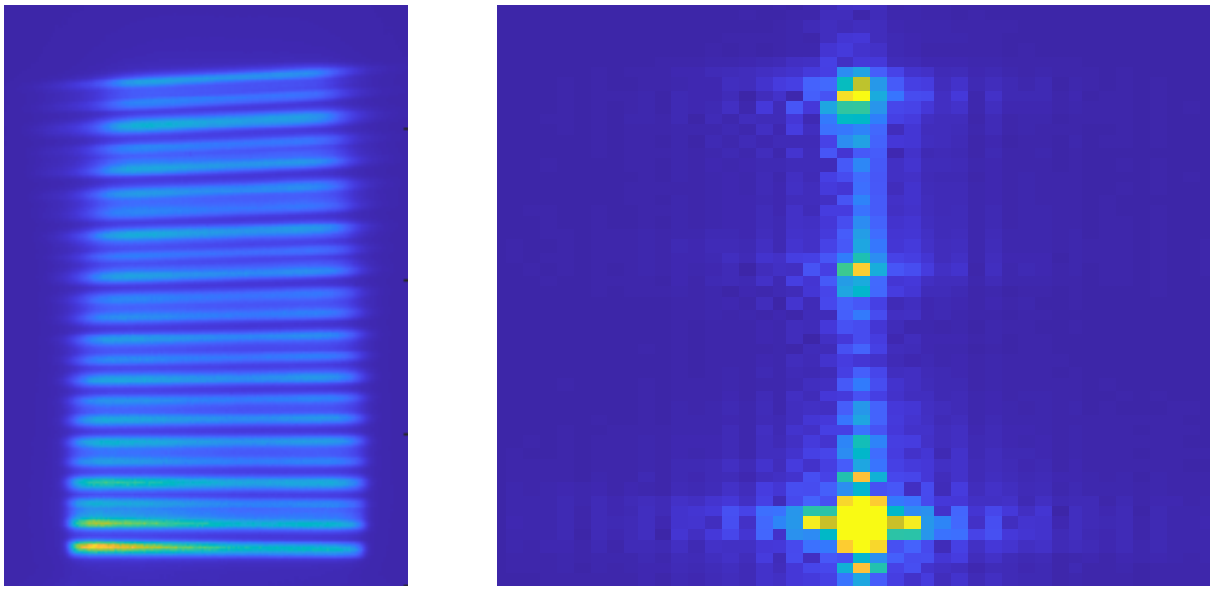

Figure 6. Left: Raw image of Hencken burner flame PLIF sheet comprising two spatial frequencies generated using the optical setup in Figure 1. Right: Fourier plane image of the PLIF sheet from the raw image. The DC signal is at the bottom of the frame, the lower-frequency portion of the PLIF sheet is displayed as the central peak in the Fourier domain, the higher spatial frequency in the Fourier domain is the peak near the top of the image.

In general, a setup where the PLIF sheet propagation vectors are not colinear is preferable from a post-processing perspective. This is because with multiple imposed spatial frequencies, the angular separation of the PLIF sheet propagation vectors lessens overlap between the signals in the Fourier plane and unwanted signal interference in processed images. Consider an example from Figure 6. Frame a) is the raw OH PLIF image of the flame with 2 imposed spatial structures. The post-processed images of this flame are shown in frames b) and c), respectively, of Figure 5. Frame b) of Figure 6 is the Fourier transform of the raw structured illumination data from frame a). The Fourier plane image has been zoomed and shifted for easier viewing such that the bright peak at the bottom of the figure corresponds to the DC signal. The peak in the center of the image corresponds to the spatial frequency imposed on the PLIF sheet from the ND6000 laser system in Figure 1, and the peak at the top of the image corresponds to the PLIF sheet with the highest spatial frequency, imposed on the beam produced by the Sirah laser system. Although the peaks are distinguishable, they appear

to have some overlap between them and it is difficult to tell where the non-zero amplitudes of frequency content associated with one peak end and where the next begins. Ideally, the regions between the two peaks would appear dark in color like those regions of the Fourier plane where frequency amplitude is lowest, such as the left and right edges of the frame, respectively. Were the propagation vectors of the laser sheets incident upon the measurement volume at larger angles to one another, they would be more easily separated within the Fourier domain via the filtering process. This is because the peak locations would be shifted left or right from one another in Fourier space and the filters employed would not accept unwanted portions of signal due to overlap of adjacent peaks.

Although reconfiguring the orientations of the beam propagation vectors would aid in filtering the various spatial frequencies compared to those in the current set up, this is not the only way to increase the distance between peaks in the Fourier domain and achieve better filtering. A simpler approach is to increase the spatial frequency of the masks in the optical setup such that the resultant spatial frequencies in the PLIF sheet are further displaced from the DC signal, and from each other, in Fourier space. Furthermore, higher spatial frequencies in the PLIF sheet images would also increase the resolution of the processed flame images. Such an optimization is important when considering applications such as two-color thermometry (discussed in the next section), which provides a quantitative measure of temperature when two PLIF images are ratioed. Utilizing the best spatial resolution possible is critical for the accuracy of such a measurement when structured illumination in employed. This is due to the measurement itself being a result of performing calculations on raw image data multiple times: first by performing a series of Fourier transforms and filter application to extract flame images, and then to ratio those extracted images to calculate a temperature.

Consider Figure 7. The left-hand image is the ratio of the reference flame images (frames c) and a), respectively) from Figure 5, and the right-hand image is the ratio of the Fourier-processed flame images (frames d) and b), respectively) also from Figure 5. Note, the right-hand ratio image is scaled by 0.75 to better match that of the reference ratio image; this is likely due to an effect of using different spatial frequencies and their input energies being scaled during the Fourier analysis process. Since the Fourier-processed images from Figure 5 are lower resolution than that of the reference image counterparts, the ratio of the processed images also has lower resolution than that of the reference images. And although the 2 images look somewhat similar, the Fourier processed ratio image displays vertical smearing compared to the reference ratio image, and it also fails to capture the finer features exhibited by the reference ratio image. Thus, improving the resolution of the Fourier-processed images by imposing higher spatial frequencies in the optical setup will be critical in acquiring accurate temperature field measurements using the two-color OH PLIF thermometry technique.

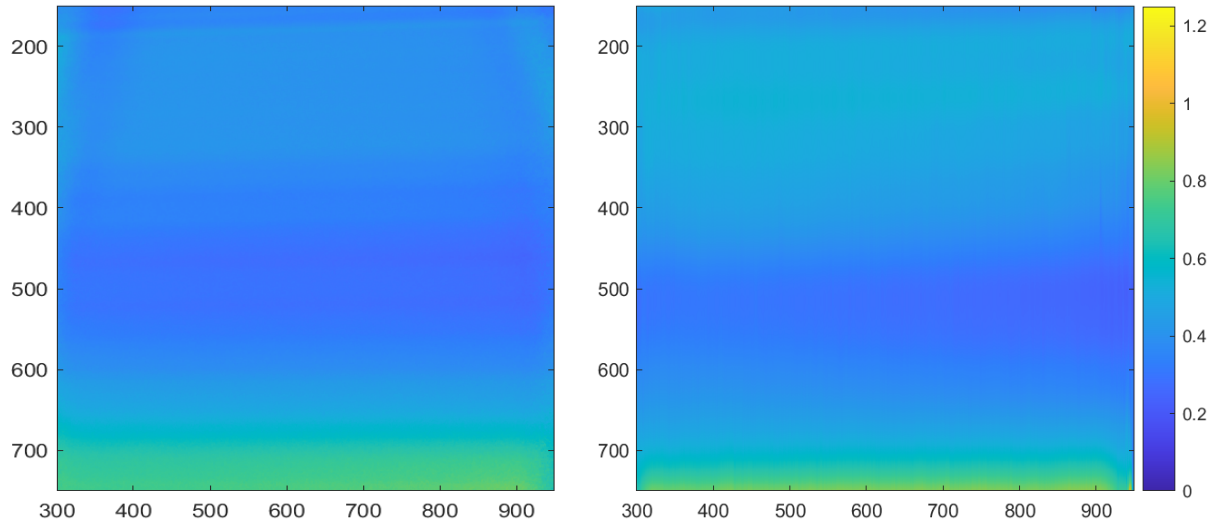

Figure 7. Ratio maps (equal color scales) of reference and Fourier-processed PLIF images, respectively, from Figure 5. Left: ratio of reference images, frame c) divided by frame a). Right: ratio of Fourier-processed images, frame d) divided by frame b). Note, the Fourier-processed ratio (right-hand frame) has been scaled by approximately 0.75 to better match that of the reference images ratio (left-hand frame).

5. Conventional OH PLIF Thermometry: Results and Discussion

As mentioned in previous sections, the structured illumination technique provides a promising means of conducting experiments in harsh environments. The ability of the technique to perform filtering of unwanted background luminosity and extraneous signals makes structured illumination a powerful tool for experimenters desiring to perform quantitative measurements in conditions previously inaccessible for such measurements. Furthermore, since the acquisition of

background frames is not required, ensemble averaging of such background is unnecessary and single-shot measurements are thus possible. Of interest to the authors, this technique is particularly promising when considering its application to a post-detonation fireball environment. In these domains, background luminosity is significant and the phenomena under investigation occur in a highly transient manner (microsecond time scale, or less), precluding background subtraction and ensemble-averaging techniques, respectively. Consequently, without the need for conventional background subtraction or long, time-averaged measurement acquisitions, a technique previously unusable in post-detonation environments can be employed; two-color OH PLIF thermometry.

To demonstrate the ability to utilize conventional two-color OH PLIF thermometry, the authors have used the optical setup described in the experimental setup section and shown in Figure 1 to record conventional two-color OH PLIF thermometry data in a Hencken burner. For these measurements, only the Sirah laser system was utilized, and no structures were imposed on the PLIF laser sheet (no masks in the setup) with an approximate PLIF sheet thickness of 0.6 mm and laser bandwidth of roughly 0.075 cm^{-1} as measured using an Angstrom/HighFinesse wavemeter (Model WF6). To collect thermometry data, the Hencken flame equivalence ratio was varied over a range of ϕ=0.60-0.75 in increments of $\Delta\phi$=0.05 using mass flow controllers. Prior to recording images for performing the PLIF thermometry technique, fluence saturation curves were recorded. Because PLIF thermometry is performed using a ratio of emitted fluorescence from two distinct excitation wavelengths, the ratio of the resultant PLIF signals of each input wavelength is equivalent to the ratio of the OH population absorbing those input wavelengths (which is unique to a particular temperature). This is only true, however, if the input fluence of each wavelength falls within the linear saturation regime of the fluence saturation curve for the OH transition of interest. To ensure that the pulse energy of the laser was within the linear PLIF regime, a series of ensemble-averaged images were recorded in the flame whereby the pulse energy was varied and compared to the resultant PLIF output signal (all images were background subtracted and corrected for flat field distortion). Let the reader recall that each PLIF image displayed herein is an average of 100 PLIF flame images recorded sequentially for each pulse of the laser system. The saturation curve of the PLIF sheet in the Hencken flame shown in Figure 8 demonstrates that the region of laser energy saturation begins at approximately 0.45 mJ/pulse for the setup in question (laser wavelength corresponding to the $Q_1(14)$ absorption line at 286.46 nm).

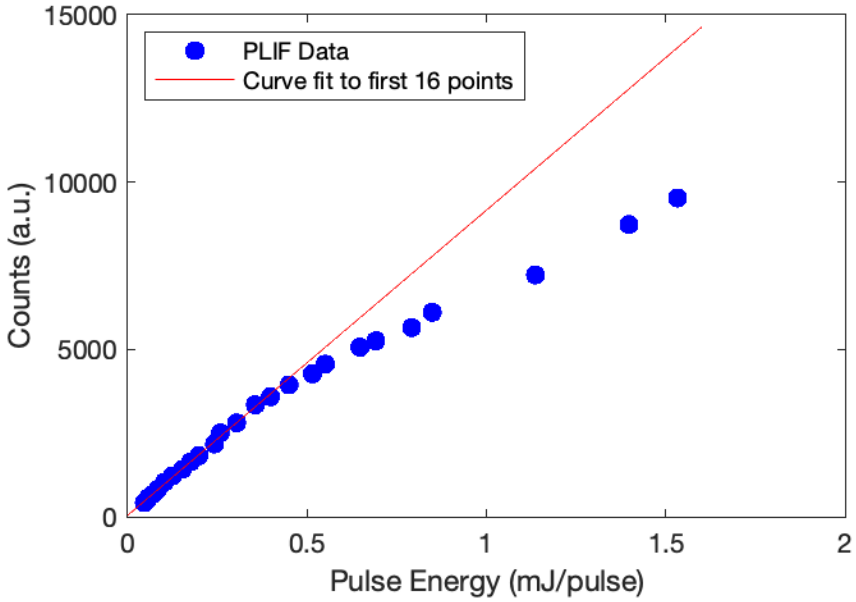

Figure 8. PLIF fluence saturation curve for $Q_1(14)$ laser sheet (286.46 nm) in the Hencken burner flame using the Sirah laser system. The PLIF signal begins to saturate at approximately 0.45 mJ/pulse. Measurements were recorded approximately 1 cm from the burner surface and 1 cm from the burner edge. Other measurement stations along the length of the burner surface and at various heights above the surface up to approximately 3 cm yielded similar results to those shown here.

After plotting the fluence saturation curve, laser pulse energies were set at approximately 0.40 mJ/pulse and separate runs of ensemble-averaged images were recorded at each equivalence ratio. At each equivalence ratio, 3 sets of PLIF flame images were recorded: 1) with no PLIF laser sheet for recording background radiation, 2) at a wavelength of 282.75 nm corresponding to the $Q_1(5)$ transition of OH and, 3) at a wavelength of 286.46 nm corresponding to the $Q_1(14)$ OH transition. Background subtraction and flat field corrections were then performed on the collected PLIF flame images, as

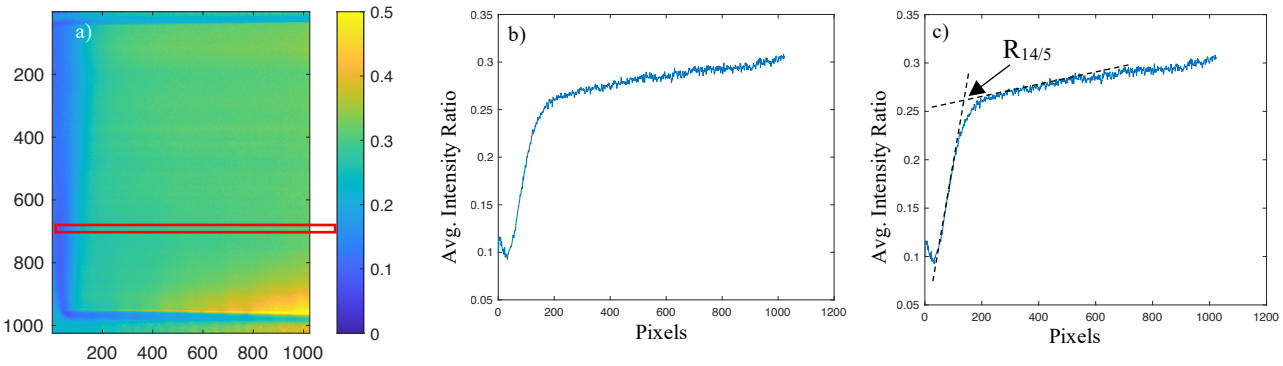

Figure 9. PLIF ratio image and plot of ratios across the flame. a) Ratio map of left-hand portion of Hencken flame where the blue-ish border near the bottom of the image corresponds to the burner surface. X- and Y-axis values are in pixel space, color axis is ratio value. The red box is the region of interest 1 cm above the flame used for analysis. b) Plot of 10-pixel vertically-averaged ratio across the flame at a height of 1 cm from burner surface. c) Location selected for defining ratio of $R_{14/5}$.

well as sheet profile corrections recorded in the dye cell within the optical setup. Next, the ratio of the $Q_1(14)$ to $Q_1(5)$ corrected PLIF images, $R_{14/5} = I_{(Q_1(14))/(Q_1(5))}$, was taken for each equivalence ratio and corrected for differences in average pulse energy for each set of images. Average pulse energies were roughly the same between image sets during data acquisition and thus only a minor correction was required corresponding to the ratio of averaged pulse energies at a given equivalence ratio.

The measurement station above the burner at which the LIF signal ratio was measured was in the near-adiabatic region of the burner, approximately 1 cm from the surface of the burner. Frame a) of Figure 9 shows the region of interest over the burner utilized for the purposes of this analysis. A strip of the ratio image which is 10 pixels high in frame a) was averaged vertically and plotted in frame b) as PLIF signal ratio vs pixel distance along the burner. It can be seen in both the image, frame a), and (more easily) in the plot in frame b), that the ratio varies as a function of distance across the flame. Similarly, the PLIF intensity emitted as the sheet traverses the flame in Figure 5 is also shown to decrease with distance. This is due to the absorption of the laser sheet as it traverses the flame: laser energy is absorbed as the beam passes through the flame, so the PLIF signal drops off following the form of the Beer-Lambert relation (an exponential decay) [31]. Because the two absorption lines of the OH population have different absorption coefficients and also different mole fractions of the total population of OH in the flame, their exponential decay behaviors differ from one another. From frame b) of Figure 9, it can be concluded that the OH population in the $Q_1(5)$ state has a larger product of absorption coefficient and concentration than that of the $Q_1(14)$ transition due to the faster falloff in intensity of the denominator of the $R_{14/5}$ ratio (previous paragraph): $Q_1(5)$ excitation light absorbed more quickly results in more light lost than the $Q_1(14)$ line, resulting in less PLIF signal and an increase in $R_{14/5}$. Additionally, were the two sheet wavelengths absorbed at the same rate (dI/dx) as they traversed the burner surface, the ratio would not vary with distance across the flame in Figure 9. This is supported from a re-examination of Figure 7. For the PLIF flame measurements shown in Figure 5 and ratioed in Figure 7, both laser systems were used, but each laser was set at an identical wavelength of 282.75 nm. Thus, the ratio results in Figure 7 are constant with distance across the flame, even if the intensities in Figure 5 are not, because each laser sheet is being absorbed at equal rates as it traverses the flame.

Due to the variation in PLIF signal ratio across the flame from absorption, a region near the flame edge was used to define the $R_{14/5}$ value for the given equivalence ratio, as shown in frame c) of Figure 9. Ideally, a correction should be performed to account for the variation in the PLIF signal across the flame and this will be discussed as part of future work. The ratio of PLIF signal intensities, $R_{14/5}$, for a given equivalence ratio (temperature) is equivalent to the ratio of populations of the $Q_1(14)$ state to that of the $Q_1(5)$ state in the (1,0) vibrational band of the $A^2\Sigma$-$X^2\Pi$ electronic transition of the OH molecule. The measured ratio results from the PLIF images at each equivalence ratio were thus converted to temperature based on the set equivalence ratio of the Hencken burner using the constant (h,p) equilibrium condition in the NASA CEA code [32]. Theoretical values of the $Q_1(14)/Q_1(5)$ LIF signal ratios were then calculated in LIFBASE [33] based on the temperature corresponding to a range of equivalence ratios. The theoretical temperatures calculated from the LIFBASE ratios were then compared to the measured PLIF temperatures in the Hencken burner and plotted against equivalence ratio. The results are given in Figure 10. It should be noted that the measured PLIF values were shifted by $\Delta\phi = +0.1$ to account for slight errors in the gas flow rates used with the Hencken burner.

Upon examining the measured PLIF temperatures compared to the theoretical LIFBASE temperatures plotted in Figure 10, reasonable agreement is shown at the equivalence ratio of $\phi = 0.7$. As the equivalence ratio increased, however, the

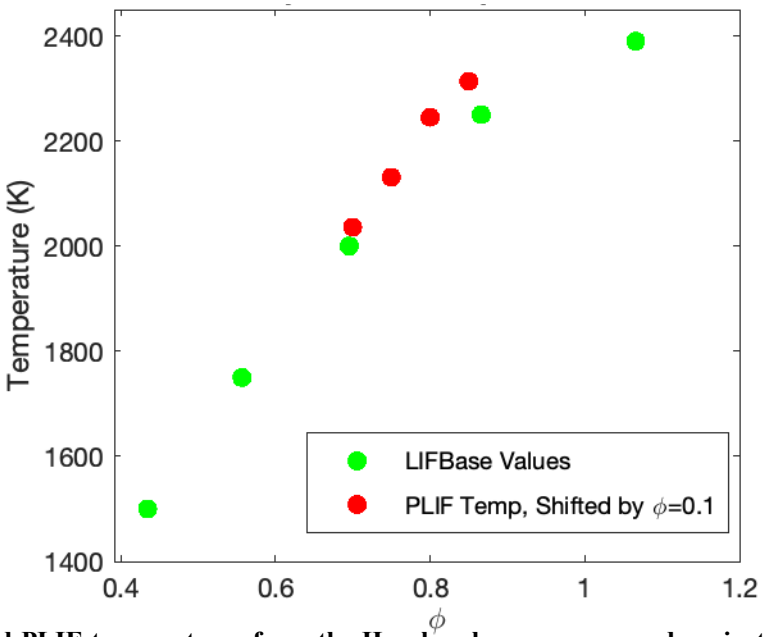

Figure 10. Measured PLIF temperatures from the Hencken burner compared against theoretical temperatures calculated from simulated LIF signal ratios in LIFBASE. The measured PLIF temperatures are shifted by Δϕ=+0.1 on the x-axis corresponding to the offset of the Hencken burner.

measured and theoretical trends begin to show greater disagreement. This is believed to be due primarily to nonideal behavior of the Hencken burner. The Hencken burner utilized in these experiments is not equipped with an inert gas co-flow around the primary fuel-oxidizer honeycomb mesh structure on the top surface of the burner. This results in the formation of a diffusion flame at the outer edges of the flame as the equivalence ratio is increased from lean to stoichiometric. In flames exhibiting an edge diffusion flame, the equivalence ratio cannot be assumed to be the same as that of the core flow of the burner, thereby altering the absorption behavior of the PLIF sheet compared to that of the uniform flame in the central region of the burner. An example of this behavior is shown in Figure 11 comparing a PLIF image without an edge diffusion flame and one with an edge diffusion flame. This behavior will be corrected as part of future work.

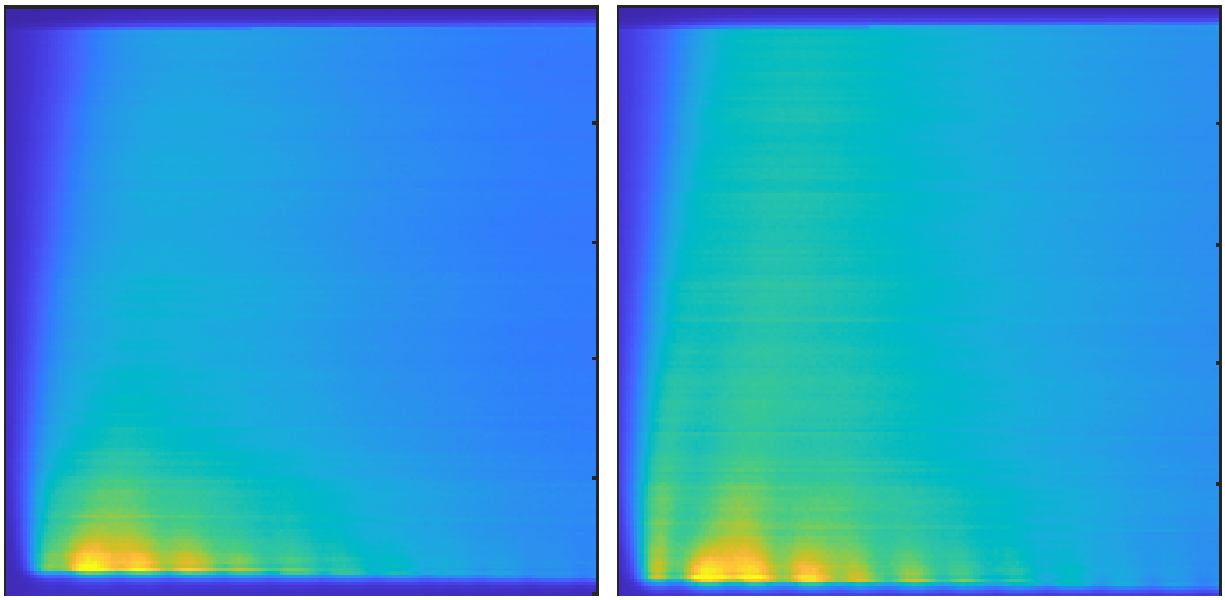

Figure 11. Two images of the left-hand side of a PLIF sheet flame from the Hencken burner. Left: image recorded at $\phi = 0.8$ exhibiting no diffusion flame behavior at the left edge of the burner. Right: image recorded at $\phi = 0.9$ exhibiting a diffusion flame at the left edge of the burner.

6. Future Work

As part of ongoing experimental work moving towards a functional thermometry setup which incorporates structured illumination, various improvements to the experimental setup are needed. For improved resolution and filtering of Fourier-processed images, higher mask spatial frequencies will likely be required. This will have a twofold benefit. First, the resolution of processed images will be improved, which is necessary for accurate temperature mapping of various flow fields. Second, higher spatial frequencies will allow for greater distance between various signals and the DC signal in the Fourier domain. The experimental setup would likely further benefit a flat flame burner configured to operate with an inert co-flow around the central flame. This will eliminate the formation of a diffusion flame at the edges of the Hencken burner flame. Upon completion of improvements to the experimental setup, an improved method for analyzing $R_{14/5}$ ratios will be implemented. Namely, a correction for absorption of the wavelengths corresponding to each PLIF sheet as they traverse the flow field need to be implemented wherein the shape of the PLIF sheet intensity decay is utilized in conjunction with the Beer-Lambert relation and known OH concentration in the flame to correct for signal attenuation across the flow field. After the above corrections and modifications are implemented, the experimental setup and analysis tools will be utilized to record two-color OH PLIF thermometry data both with and without the inclusion of the structured illumination technique as a means of validating the structured PLIF thermometry diagnostic. Finally, the structured PLIF thermometry diagnostic will be used to collect thermometry data in post-detonation environments.

7. Conclusion

The structured illumination technique has been applied to the collection of data in a canonical Hencken burner flame for describing the mechanics and utility of the technique when applied to OH PLIF. After describing the basics of structured illumination, examples of the method for post-processing images recorded with imposed spatial frequencies were provided, along with demonstrations of filtering unwanted background signals and separating multiple spatial frequencies from images recorded with a single detector, respectively. A demonstration of two-color OH PLIF thermometry was then provided, along with a discussion of the benefits of utilizing the structured illumination technique in conjunction with a two-color OH PLIF diagnostic in highly transient and highly luminous environments, such as those of a post-detonation fireball. Lastly a brief discussion was provided regarding future work for the continued development of the implementation of structured OH PLIF thermometry.

Acknowledgments

Support of the Laboratory Directed Research and Development (LDRD) program at Sandia National Laboratories is gratefully acknowledged. Sandia National Laboratories is a multimission laboratory managed and operated by National Technology & Engineering Solutions of Sandia, LLC, a wholly owned subsidiary of Honeywell International Inc., for the U.S. Department of Energy's National Nuclear Security Administration under contract DE-NA0003525. This paper describes objective technical results and analysis. Any subjective views or opinions that might be expressed in the paper do not necessarily represent the views of the U.S. Department of Energy or the United States Government.

References

1. Austin, J. M., Pintgen, F., and Shepherd, J. E. "Reaction zones in highly unstable detonations," *Proceedings of the Combustion Institute* Vol. 30, No. 2, 2005, pp. 1849-1857.
doi: 10.1016/j.proci.2004.08.157

2. Boeck, L. R., Mével, R., Fiala, T., Hasslberger, J., and Sattelmayer, T. "High-speed OH-PLIF imaging of deflagration-to-detonation transition in H2–air mixtures," *Experiments in Fluids* Vol. 57, No. 6, 2016.
doi: 10.1007/s00348-016-2191-z

3. Cho, K. Y., Fugger, C. A., Fievisohn, R. T., Sell, B., Hoke, J., Kearney, S. P., Caswell, A. W., Gord, J. R., and Schauer, F. "Burst-mode 355 nm PLIF for Detonation Wave Front Visualization and 100–300 kHz Particle Image Velocimetry," *AIAA Scitech 2019 Forum*. 2019.

4. Pintgen, F., Eckett, C. A., Austin, J. M., and Shepherd, J. E. "Direct observations of reaction zone structure in propagating detonations," *Combustion and Flame* Vol. 133, No. 3, 2003, pp. 211-229.
doi: 10.1016/s0010-2180(02)00458-3

5. Rankin, B. A., Fugger, C. A., Richardson, D. R., Cho, K. Y., Hoke, J., Caswell, A. W., Gord, J. R., and Schauer, F. "Evaluation of Mixing Processes in a Non-Premixed Rotating Detonation Engine Using Acetone PLIF," *54th AIAA Aerospace Sciences Meeting*. 2016.

6. Berrocal, E., Pettersson, S. G., and Kristensson, E. "High-contrast imaging through scattering media using structured illumination and Fourier filtering," *Opt Lett* Vol. 41, No. 23, 2016, pp. 5612-5615.
doi: 10.1364/OL.41.005612

7. Chartier, C., Sjoholm, J., Kristensson, E., Andersson, O., Richter, M., Johansson, B., and Alden, M. "Air-Entrainment in Wall-Jets Using SLIPI in a Heavy-Duty Diesel Engine," *SAE International Journal of Engines* Vol. 5, No. 4, 2012, pp. 1684-1692.
doi: 10.4271/2012-01-1718

8. Dorozynska, K., Kornienko, V., Alden, M., and Kristensson, E. "A versatile, low-cost, snapshot multidimensional imaging approach based on structured light," *Opt Express* Vol. 28, No. 7, 2020, pp. 9572-9586.
doi: 10.1364/OE.384535

9. Dorozynska, K., and Kristensson, E. "Implementation of a multiplexed structured illumination method to achieve snapshot multispectral imaging," *Opt Express* Vol. 25, No. 15, 2017, pp. 17211-17226.
doi: 10.1364/OE.25.017211

10. Kempema, N. J., and Long, M. B. "Quantitative Rayleigh thermometry for high background scattering applications with structured laser illumination planar imaging," *Appl Opt* Vol. 53, No. 29, 2014, pp. 6688-97.
doi: 10.1364/AO.53.006688

11. Kristensson, E., and Berrocal, E. "Crossed patterned structured illumination for the analysis and velocimetry of transient turbid media," *Sci Rep* Vol. 8, No. 1, 2018, p. 11751.
doi: 10.1038/s41598-018-30233-y

12. Kristensson, E., Berrocal, E., Wellander, R., Ritcher, M., Aldén, M., and Linne, M. "Structured illumination for 3-D Mie imaging and 2-D attenuation measurements in optically dense sprays," *Proceedings of the Combustion Institute* Vol. 33, No. 1, 2011, pp. 855-861.
doi: 10.1016/j.proci.2010.06.016

13. Kristensson, E., Ehn, A., Bood, J., and Aldén, M. "Advancements in Rayleigh scattering thermometry by means of structured illumination," *Proceedings of the Combustion Institute* Vol. 35, No. 3, 2015, pp. 3689-3696.
doi: 10.1016/j.proci.2014.06.056

14. Kristensson, E., Li, Z., Berrocal, E., Richter, M., and Aldén, M. "Instantaneous 3D imaging of flame species using coded laser illumination," *Proceedings of the Combustion Institute* Vol. 36, No. 3, 2017, pp. 4585-4591.
doi: 10.1016/j.proci.2016.08.040

15. Kulkarni, A. P., and Deshmukh, D. "Planar liquid volume fraction measurements in air-blast sprays using SLIPI technique with numerical corrections," *Applied Physics B* Vol. 124, No. 9, 2018.
doi: 10.1007/s00340-018-7057-z

16. Larsson, K., Jonsson, M., Borggren, J., Kristensson, E., Ehn, A., Alden, M., and Bood, J. "Single-shot photofragment imaging by structured illumination," *Opt Lett* Vol. 40, No. 21, 2015, pp. 5019-22.
doi: 10.1364/OL.40.005019

17. Mishra, Y. N., Boggavarapu, P., Chorey, D., Zigan, L., Will, S., Deshmukh, D., and Rayavarapu, R. "Application of FRAME for Simultaneous LIF and LII Imaging in Sooting Flames Using a Single Camera," *Sensors (Basel)* Vol. 20, No. 19, 2020.
doi: 10.3390/s20195534

18. Mishra, Y. N., Kristensson, E., Koegl, M., Jönsson, J., Zigan, L., and Berrocal, E. "Comparison between two-phase and one-phase SLIPI for instantaneous imaging of transient sprays," *Experiments in Fluids* Vol. 58, No. 9, 2017. doi: 10.1007/s00348-017-2396-9

19. Scotte, C., Sivankutty, S., Stockton, P., Bartels, R. A., and Rigneault, H. "Compressive Raman imaging with spatial frequency modulated illumination," *Opt Lett* Vol. 44, No. 8, 2019, pp. 1936-1939. doi: 10.1364/OL.44.001936

20. Zentgraf, F., Stephan, M., Berrocal, E., Albert, B., Böhm, B., and Dreizler, A. "Application of structured illumination to gas phase thermometry using thermographic phosphor particles: a study for averaged imaging," *Experiments in Fluids* Vol. 58, No. 7, 2017. doi: 10.1007/s00348-017-2364-4

21. Grisch, F., and Orain, M. "Role of Planar Laser-Induced Fluorescence in Combustion Research," *AerospaceLab*, No. 1, 2009, pp. p. 1-14.

22. Hanson, R. K. "Combustion diagnostics: Planar imaging techniques," *Symposium (International) on Combustion* Vol. 21, No. 1, 1988, pp. 1677-1691. doi: https://doi.org/10.1016/S0082-0784(88)80401-6

23. Hanson, R. K., Seitzman, J. M., and Paul, P. H. "Planar laser-fluorescence imaging of combustion gases," *Applied Physics B* Vol. 50, No. 6, 1990, pp. 441-454. doi: 10.1007/BF00408770

24. Loe, C. M., Winner, J. D., and Sánchez-González, R. "Thermometry in gas flows using two-line fluorescence imaging and structured illumination," *OSA Continuum* Vol. 1, No. 4, 2018. doi: 10.1364/osac.1.001185

25. Kornienko, V., Kristensson, E., Ehn, A., Fourriere, A., and Berrocal, E. "Beyond MHz image recordings using LEDs and the FRAME concept," *Sci Rep* Vol. 10, No. 1, 2020, p. 16650. doi: 10.1038/s41598-020-73738-1

26. Li, Z., Borggren, J., Berrocal, E., Ehn, A., Aldén, M., Richter, M., and Kristensson, E. "Simultaneous multispectral imaging of flame species using Frequency Recognition Algorithm for Multiple Exposures (FRAME)," *Combustion and Flame* Vol. 192, 2018, pp. 160-169. doi: 10.1016/j.combustflame.2018.02.009

27. Jiang, N., Hsu, P. S., Grib, S. W., and Roy, S. "Simultaneous high-speed imaging of temperature, heat-release rate, and multi-species concentrations in turbulent jet flames," *Opt Express* Vol. 27, No. 12, 2019, pp. 17017-17026. doi: 10.1364/OE.27.017017

28. Ravikrishna, R. V., and Sahu, A. B. "Advances in understanding combustion phenomena using non-premixed and partially premixed counterflow flames: A review," *International Journal of Spray and Combustion Dynamics* Vol. 10, No. 1, 2017, pp. 38-71. doi: 10.1177/1756827717738168

29. Guildenbecher, D. R., Dallman, A. R., Hall, E. M., Halls, B. R., Jones, E. M. C., Kearney, S. P., Marinis, R. T., Murzyn, C., Richardson, D. R., Perez, F., Reu, P. L., Thompson, A. D., Welliver, M. C., Mazumdar, E. C., Pourpoint, T. L., White, C. M. L., Brown, A. D., Balachandar, S., and Houim, R. W. "Advancing the science of explosive fragmentation and afterburn fireballs though experiments and simulations at the benchtop scale." United States, 2020.

30. Richardson, D. R., Kearney, S. P., and Guildenbecher, D. R. "Post-detonation fireball thermometry via femtosecond-picosecond coherent anti-Stokes Raman Scattering (CARS)," *Proceedings of the Combustion Institute* Vol. 38, No. 1, 2021, pp. 1657-1664. doi: 10.1016/j.proci.2020.06.257

31. Kostka, S., Roy, S., Lakusta, P. J., Meyer, T. R., Renfro, M. W., Gord, J. R., and Branam, R. "Comparison of line-peak and line-scanning excitation in two-color laser-induced-fluorescence thermometry of OH," *Applied Optics* Vol. 48, No. 32, 2009, pp. 6332-6343.
doi: 10.1364/AO.48.006332

32. McBride, B. J., and Gordon, S. "Computer Program for Calculation of Complex Chemical Equilibrium Compositions and Applications." NASA, 1996.

33. Luque, J., and Crosley, D. R. "LIFBASE, Database and Spectral SImulation for Diatomic Molecules (v 1.6)." SRI International, 1999.